Overview of probe diagnostics on the H-1 heliac

D. L. Rudakov,[a] M. G. Shats, R. W. Boswell, C. Charles, and J. Howard
Plasma Research Laboratory, Research School of Physical Sciences and Engineering, Australian National University, Canberra ACT 0200, Australia

(Presented on 8 June 1998)

A complex of probe diagnostics allows extensive characterization of the plasma parameters in the H-1 heliac. The probes used on H-1 include quadruple probes, poloidal and radial ''fork'' probes, a Mach probe, a 24-channel probe array, and a retarding field energy analyzer. This article provides details of the probe design and a brief description of the experimental techniques involved. Different techniques are compared. Sample results in two different modes of confinement in H-1 are presented. The capabilities of the probe diagnostics used in different combinations are discussed. © *1999 American Institute of Physics.* [S0034-6748(99)52201-6]

I. INTRODUCTION

Probes are among the most basic plasma diagnostics. They are generally simple in construction and use, relatively inexpensive, and robust enough to withstand considerable heat fluxes. They have excellent spatial resolution, limited only by the probe size and by the accuracy of the positioning mechanism. Electric or Langmuir probes[1] can provide measurements of such basic plasma parameters as electron density n_e, electron temperature T_e, and plasma potential V_p. Good temporal resolution make electric probes a useful tool in plasma fluctuation studies.

H-1[2,3] is a three-field-period toroidal heliac with a major radius $R=1.0$ m and an average minor radius $\bar{a}\approx 0.15$ m, currently operating at low magnetic fields $B_0=0.04-0.15$ T. Plasma is created and sustained by up to 100 kW of radio frequency (rf) power at 7 MHz with the pulse duration of 30–80 ms. The typical argon plasma parameters are: line average electron density $\bar{n}_e\sim 0.5-1\times 10^{18}$ m^{-3}, central electron temperature $T_e(0)\sim 7-30$ eV, and central ion temperature $T_i(0)\sim 40-150$ eV. These experimental conditions allow extensive use of probes throughout the plasma cross section. The probes used on H-1 include single probes, a quadruple probe, symmetric and asymmetric double-quadruple ''fork'' probes, a Mach probe, and a 24-channel probe array, as well as a retarding field energy analyzer (RFEA). Used simultaneously in a number of different combinations these probes allow measurements of the most basic plasma parameters, their radial gradients, and fluctuations.

II. PROBE DESIGN

Most of the Langmuir probes used on H-1 have similar construction. Figure 1 shows the design of the quadruple probe (a), Mach probe (b), and 24-pin probe array (c). The probes are made of 0.8 mm tungsten wire inserted through the bores in alumina insulators. Spacers wound with thin copper wire are located inside the bores about 10 mm from the probe tips to ensure that the tips do not touch the edges of the bores. This is necessary to prevent current leakage between the tips or an increase in the effective collecting area of the probes due to sputtered material being deposited on the alumina edge facing the plasma. The Mach probe has a barrier between the two tips to make them direction sensitive. All probes have stainless steel shields to prevent rf pick-up. Electric connections to the tungsten wires are made with sliding contacts clamped to Teflon-coated copper wires laid inside radially movable vacuum drives. Two quadruple probes can be installed on a single drive to form either a poloidal or a radial fork probe. In a poloidal fork probe two quadruple probes are of the same length, separated by 15 mm in the poloidal direction. In a radial fork probe the probe tips are separated by 15 mm in both poloidal and radial directions.

III. RFEA DESIGN AND BIASING

The design of the RFEA[4] is schematized in Fig. 2(a). The analyzer consists of four grids and a collector plate. The

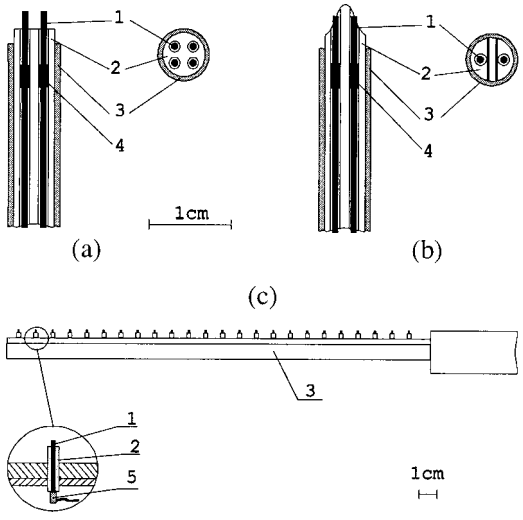

FIG. 1. Probe design: quadruple probe (a), Mach probe (b), 24-pin probe array (c). 1: tungsten wire, 2: alumina insulator, 3: stainless steel shield, 4: spacer, 5: sliding contact clamped to Teflon-coated copper wire.

[a]Electronic mail: dlr112@rsphysse.anu.edu.au

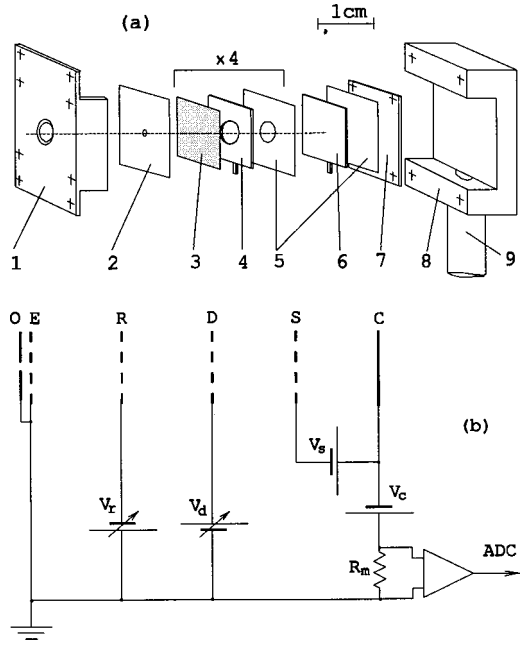

FIG. 2. RFEA design (a) and biasing (b). 1—analyzer lid, 2—orifice plate, 3—Ni mesh, 4—copper support plate, 5—mica insulators, 6—collector, 7—clamp plate, 8—analyzer body, 9—support tube, *O*—orifice plate, *E*—entrance grid, *R*—repeller grid, *D*—discriminator grid, *S*—suppressor grid, *C*—collector.

grids made of 812 rule Ni mesh are supported by the copper plates separated by mica insulators. The grid stack is assembled on the analyzer lid and is held together by a clamp plate. Plasma particles enter the analyzer through a 2 mm hole in a 0.1 mm thick stainless steel orifice plate. The entrance grid and the orifice plate are in electrical contact with the analyzer lid, which is connected to the grounded vacuum vessel of H-1.

The analyzer biasing circuit in the ion mode of operation is shown in Fig. 2(b). The grounded entrance grid (*E*) serves to ensure the continuity of the sheath potential surface across the front of the probe while allowing the input hole in the orifice plate (*O*) to be made sufficiently large to provide enough current at low plasma densities. The repeller grid (*R*) serves to repel the plasma electrons and is biased from an external adjustable dc power supply at $V_r \leqslant -100$ V. The discriminator grid (*D*) serves to retard the plasma ions allowing only those with sufficient parallel energy $E_{\|} > eV_d$ to reach the collector (*C*). This grid can be biased from either an adjustable dc power supply [as shown in Fig. 2(b)] or a high voltage amplifier. The secondary electron emission control (suppressor) grid (*S*) is biased negatively with respect to the collector (*C*) at $V_s = -9$ V to suppress the secondary electron current from the collector. The collector itself has a negative bias with respect to ground, $V_c = -9$ V. Both the suppressor grid and the collector are biased from fixed voltage batteries. The collector current is monitored across a measuring resistor $R_m = 10\ \mathrm{k}\Omega$. A variable gain ($G = 1-1000$) buffer amplifier allows the current measurements to be done within a wide range of plasma densities without changing the measuring resistor.

IV. MEASUREMENTS OF THE BASIC PLASMA PARAMETERS

The electron density n_e, electron temperature T_e, and plasma potential V_p are inferred from single and triple probe data as:[1,5,6]

$$n_e = \frac{2I_{si}}{ec_sA_p} = 2\frac{I_{\mathrm{si}}}{eA_p}\sqrt{\frac{m_i}{k(ZT_e+T_i)}}, \tag{1}$$

$$\frac{kT_e}{e} = \frac{(V_+ - V_f)}{\ln 2}, \tag{2}$$

$$V_p = V_f - \frac{1}{2}\ln\left[2\pi\frac{m_e}{m_i}\left(1+\frac{T_i}{T_e}\right)(1-\delta)^{-2}\right]\frac{kT_e}{e}, \tag{3}$$

where I_{si} is the ion saturation current, $c_s = \sqrt{k(ZT_e+T_i)/m_i}$ is the ion acoustic velocity, A_p is the probe collecting area, Z is the ion charge state (typically $Z=1$ in H-1), k is the Boltzmann constant, e is the electron charge, m_e, m_i, T_e, and T_i are the electron and ion masses and temperatures, respectively, V_f is the floating potential, V_+ is the potential of the positive pin of a triple probe, and δ is the secondary electron emission coefficient. For the typical experimental conditions in H-1 (in argon)

$$V_p \approx V_f + 4\frac{kT_e}{e}. \tag{4}$$

Time-resolved measurements of the radial gradients of n_e, T_e, and V_p (E_r) are performed with the radial fork probe. Another quadruple probe is located in the adjacent cross section and is typically fixed at about the last closed flux surface (LCFS). This arrangement allows measurements of both local (across 15 mm) and average (from $r/a \approx 1$ to $r/a \approx 0.3$) gradients of the plasma parameters.

The ion temperature T_i is measured by the RFEA. For a Maxwellian velocity distribution the dependence of the collector current I_c on the discriminator voltage V_d is given by[7–9]

$$I_c = I_{c0}, \quad V_d \leqslant V_p, \tag{5a}$$

$$I_c = I_{c0}\exp\left(\frac{-Ze(V_d - V_p)}{KT_i}\right), \quad V_d \geqslant V_p. \tag{5b}$$

The ion temperature can be determined by performing a least-square fit of Eq. (5b) to a measured $I_c(V_d)$ characteristic. The plasma potential can be determined from a knee on the characteristic. The accuracy of the potential measurements is, however, limited to ~10 V, since the knee is rounded due to the acceptance angle limitation of the analyzer.

V. FLUCTUATION STUDIES

The use of quadruple probes allows simultaneous continuous measurements of the local values of the ion saturation current I_{si}, the floating potential V_f, and the electron temperature T_e. The fluctuating components of the electron density $\tilde{n}_e$, electron temperature $\tilde{T}_e$, and plasma potential

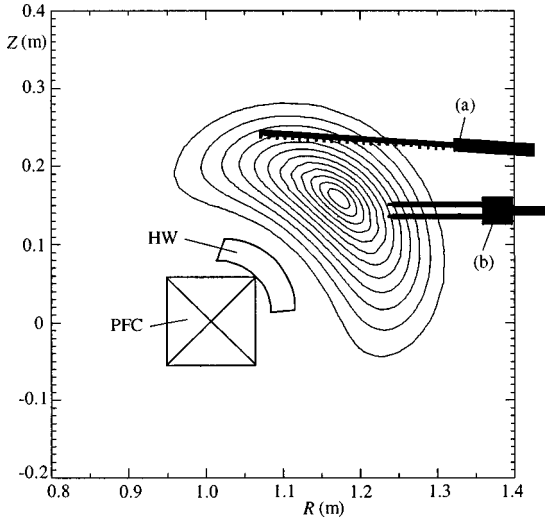

FIG. 3. Schematic of k_θ measurements with the 24-pin probe array (a) or the poloidal fork probe (b).

$\tilde{V}_p$ can be inferred using Eqs. (1)–(4). This allows for an experimental estimate of the fluctuation-driven radial particle flux[6]

$$\Gamma_\perp^{\mathrm{fl}} = \frac{1}{B}\langle \tilde{n}\tilde{E}_\theta \rangle = \frac{k_\theta}{B}\langle \tilde{n}\tilde{V}_p \rangle, \tag{6}$$

where k_θ is the poloidal wave number of the fluctuation and $\langle\rangle$ denotes a cross correlation between the density and the electric field (or the potential) fluctuations. This cross correlation can be obtained by applying digital spectral analysis methods[10] to $\tilde{n}_e$ and $\tilde{V}_p$ signals inferred from the quadruple probe data.

As have been previously reported,[11–13] the fluctuations in H-1 are global, highly coherent, and have low poloidal mode numbers $m=1-2$. Consequently, the fluctuation wavelength is much larger than the separation of the tips of the quadruple probe ($\sim$1.5 mm). This is an advantage when determining $\langle \tilde{n}\tilde{V}_p \rangle$, since the spatial resolution of the method is not compromised. However, this separation is not sufficient to reliably measure k_θ. Measurements of k_θ are therefore performed either by the 24-pin probe array inserted into the plasma tangentially or by the symmetric fork probe, as shown in Fig. 3.

VI. MEASUREMENTS OF THE ION FLOW VELOCITIES

The ion fluid flow velocities are measured with the Mach probe.[14,15] Under the typical experimental conditions in H-1 the characteristic probe size ($r_p \sim 1$ mm) is much smaller than the ion Larmor radius ($r_{\mathrm{Li}} \approx 2-6$ cm in argon). Therefore, we use an ''unmagnetized'' theory of Hudis and Lidsky[16] (modified slightly for the case $T_i \geqslant T_e$) for the interpretation of the Mach probe data in H-1. This theory gives the following relationship between the Mach number of the flow M and the ratio of the currents to the tips of the Mach probe:

$$M \equiv \frac{v_d}{c_s} = \frac{1}{4}\sqrt{\frac{ZT_e + T_i}{T_i}}\ln\left(\frac{I_{\mathrm{si}}^+}{I_{\mathrm{si}}^-}\right), \tag{7}$$

where v_d is the flow velocity, c_s is the ion acoustic velocity, Z is the ion charge state, and I_{si}^+, I_{si}^- are the ion saturation currents to the tips facing upstream (+) and downstream (−), respectively.

VII. CROSS CALIBRATION OF DIFFERENT TECHNIQUES

In many cases the plasma parameters were measured using more than one technique. For example, in addition to the triple probe measurements, the electron temperature was measured using single probes swept at 50 Hz [by performing a least-square exponential fit to the measured current–voltage ($I-V$) characteristic[6]] and at 50 kHz (by the ratio of the first and second current harmonics[17]). All three methods were found to be in good agreement everywhere inside the LCFS. The triple probe technique was chosen for the routine measurements, since for the same temporal resolution it has lower requirements to the analog-to-digital converter (ADC) sampling rate than the swept probe techniques.

The plasma potential was measured using triple probes as well as RFEA. The results generally agreed within the accuracy of the measurements. Of the two methods the triple probe technique has much better temporal resolution and higher accuracy, so it was employed more often.

The electron density measurements done with single probes were calibrated against the 8 mm microwave interferometer data to eliminate the effect of the finite sheath thickness on the effective collecting area of the probes. Since the two methods agreed well without any correction, the probe area enlargement by the sheath was presumed negligible inside the LCFS.

Finally, the ion temperature and the ion poloidal flow velocity measurements made with the RFEA and Mach probe, respectively, were compared to the results obtained from the modulated solid state (MOSS) spectrometer.[18] The results showed satisfactory agreement (within the accuracy of the measurements).

VIII. EXPERIMENTAL RESULTS

The bulk of the experimental results so far obtained using the techniques described above have been reported elsewhere.[11–13,19,20] Figure 4 presents some sample results in two different modes of confinement in H-1. Shown are the radial profiles (measured on a shot-to-shot basis) of the electron density (a), relative density fluctuations (b), fluctuation-induced particle flux (c), plasma potential (d), ion temperature (e), and poloidal ion flow velocity (f) in L (diamonds) and H (squares) modes. The data were taken in a few series of shots in argon under similar operational conditions: filling pressure $P_{\mathrm{fill}} \approx 3\times 10^{-5}$ Torr, rf heating power $P_{\mathrm{rf}} \approx 85$ kW, magnetic field at the axis $B_0 \approx 0.06$ T (L mode) and $B_0 \approx 0.075$ T (H mode). Figure 4 illustrates most of the characteristic features of the H mode with respect to the L mode in H-1:[12,19,20] increase in the central plasma density and density gradient (a); suppression of the fluctuations (b), and associated particle flux (c); decrease of the central

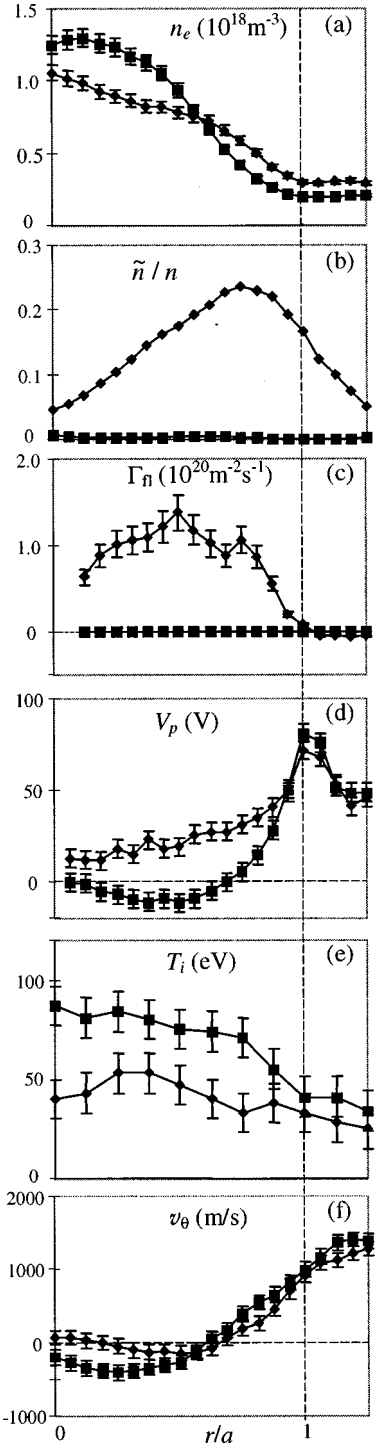

FIG. 4. Radial profiles of the electron density (a), relative density fluctuations (b), fluctuation-induced particle flux (c), plasma potential (d), ion temperature (e), and poloidal ion flow velocity (f) in *L* (diamonds) and *H* (squares) modes.

plasma potential and increase in the radial electric field (d); increase in the ion temperature (e); no significant changes in the ion poloidal flow velocity (f).

The extensive characterization of the plasma parameters in H-1 is possible due to the simultaneous use of a number of probes. For example, determination of the electron density from the ion saturation current requires measurements of both the electron and the ion temperatures [see Eq. (1)]. The same requirement stands for the ion flow velocity measurements with the Mach probe [Eq. (7)]. In our experiments this requirement is satisfied by using a quadruple probe, a Mach probe, and RFEA simultaneously (or under similar conditions). Another example is the measurement of the fluctuation-driven particle flux, which requires simultaneous time-resolved measurements of the electron density, plasma potential, and the poloidal wave number of the fluctuations. This is realized by simultaneously using either two quadruple probes (combined in a poloidal fork probe) or a single quadruple probe and a 24-pin probe array.

IX. DISCUSSION

Probe diagnostics proved to be very useful during the first stage of operation of the H-1 heliac. The bulk of the data pertaining to the improved confinement mode in H-1 was obtained using probe techniques. Although most individual techniques used on H-1 are well known, the combined use of a number of different methods allows more extensive characterization of the plasma parameters than usually achieved in comparable experiments.

[1] N. Hershkowitz, *Plasma Diagnostics: Discharge Parameters and Chemistry* (Academic, New York, 1989), p. 131.
[2] S. M. Hamberger, B. D. Blackwell, L. E. Sharp, and D. B. Shenton, Fusion Technol. **17**, 123 (1990).
[3] M. G. Shats, D. L. Rudakov, B. D. Blackwell, L. E. Sharp, R. Tumlos, S. M. Hamberger, and O. I. Fedyanin, Nucl. Fusion **34**, 1653 (1994).
[4] G. D. Conway and A. J. Perry, ANU-PRL-TR-02/96, Plasma Research Laboratory, Australian National University, Canberra, ACT (1996).
[5] S.-L. Chen and T. Sekiguchi, J. Appl. Phys. **36**, 2363 (1965).
[6] P. C. Stangeby and G. M. McCracken, Nucl. Fusion **30**, 1225 (1990).
[7] G. F. Matthews, J. Phys. D **17**, 2243 (1984).
[8] A. S. Wan, T. F. Young, B. Lipschultz, and B. LaBombard, Rev. Sci. Instrum. **57**, 1542 (1986).
[9] C. Bohm and J. Perrin, Rev. Sci. Instrum. **64**, 31 (1993).
[10] E. J. Powers, Nucl. Fusion **14**, 749 (1974).
[11] M. G. Shats, B. D. Blackwell, G. G. Borg, S. M. Hamberger, J. Howard, D. L. Rudakov, and L. E. Sharp, Trans. Fusion Technol. **27**, 286 (1995).
[12] M. G. Shats, D. L. Rudakov, B. D. Blackwell, G. G. Borg, R. L. Dewar, S. M. Hamberger, J. Howard, and L. E. Sharp, Phys. Rev. Lett. **77**, 4190 (1996).
[13] M. G. Shats and D. L. Rudakov, Phys. Rev. Lett. **79**, 2690 (1997).
[14] P. C. Stangeby, Phys. Fluids **27**, 2699 (1984).
[15] B. J. Peterson, J. N. Talmadge, D. T. Anderson, F. S. B. Anderson, and J. L. Shohet, Rev. Sci. Instrum. **65**, 2599 (1994).
[16] M. Hudis and L. M. Lidsky, J. Appl. Phys. **41**, 5011 (1970).
[17] R. Van Nieuwenhove and G. Van Ost, Rev. Sci. Instrum. **59**, 1053 (1988).
[18] J. Howard, Rev. Sci. Instrum. (these proceedings).
[19] M. G. Shats, D. L. Rudakov, R. W. Boswell, and G. G. Borg, Phys. Plasmas **4**, 3629 (1997).
[20] M. G. Shats, C. A. Michael, D. L. Rudakov, and B. D. Blackwell, Phys. Plasmas **5**, 2390 (1998).